Vibration Reduction of Coaxial Rotor by Blade Installation Phase Angle

Takumi Yumino, t-yumino@st.go.tuat.ac.jp, Tokyo University of Agriculture and Technology (Japan)
Hideaki Sugawara, sugawara.hideaki@jaxa.jp, Japan Aerospace Exploration Agency (Japan)
Yasutada Tanabe, tan@jaxa.jp, Japan Aerospace Exploration Agency (Japan)
Masaharu Kameda, kame@cc.tuat.ac.jp, Tokyo University of Agriculture and Technology (Japan)

Abstract

Aerodynamic lift variations of an isolated coaxial rotor system were analyzed by a computational fluid dynamics (CFD) approach. The study focused on a coaxial rotor configuration equipped with four blades per rotor and employed rFlow3D, a CFD solver specifically tailored for rotorcraft analyses. The analysis focuses on the high-speed forward flight with an advance ratio of 0.6 or higher, which is the ratio of the forward speed to the rotor tip speed. The numerical findings demonstrate a significant reduction in lift variation and reveal that the appropriate inter-rotor phase angle holds the potential to minimize the fluctuation to a level akin to that experienced during hovering. This reduction can be attributed to the mitigation of the vibrational component associated with the number of blades per rotor revolution. A detailed analysis further reveals that the pitching and rolling moments exhibit opposing changes in response to variations in the inter-rotor phase angle.

1. BACKGROUND

Helicopters play a pivotal role in contemporary society owing to their exceptional hovering capabilities. Among the various applications of helicopters, life-saving activities stand out, necessitating swift patient transportation. Nonetheless, present-day helicopters encounter challenges in achieving high-speed flight due to the substantial disparity in airspeed between the advancing and retreating side blades. To address this, contemporary helicopters implement swash-plates to periodically adjust the pitch angle, thereby maintaining rolling moment equilibrium between the advancing and retreating sides. Nevertheless, this configuration results in inadequate overall rotor thrust, rendering high-speed flights, such as those reaching 500 km/h, unfeasible.

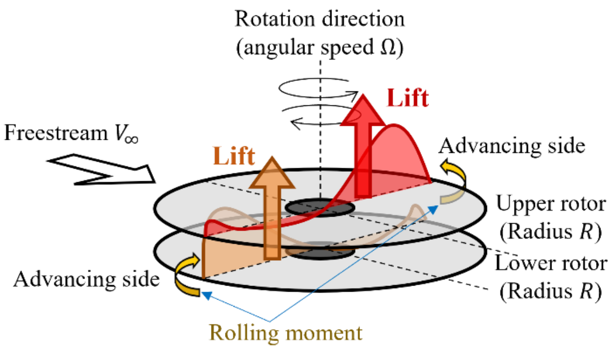

Figure 1: Coaxial rotor system with lift offset.

The compound helicopter embodies a concept aimed at increasing the velocity capabilities of rotorcraft (Ref. 1). It comprises distinct lift-generating and propulsion-generating mechanisms. Among these concepts is the coaxial helicopter, featuring a rotor system comprising a pair of counter-rotating rotors, as depicted in Figure 1. The coaxial rotor configuration generates greater lift on the advancing side than on the retreating side, thereby providing sufficient lift for high-speed flight. Additionally, the rolling and yawing moments are nullified by the opposing rotation directions of the upper and lower rotors.

Sikorsky, a prominent U.S. company, has denominated this concept as the "Advancing Blade Concept (Ref. 2)" and has developed a demonstrator aircraft, the X2 Technology Demonstrator, which has attained an impressive flight speed of 463 km/h (Ref. 3). Key parameters in this concept is the "lift offset," a pivotal parameter defined as follows:

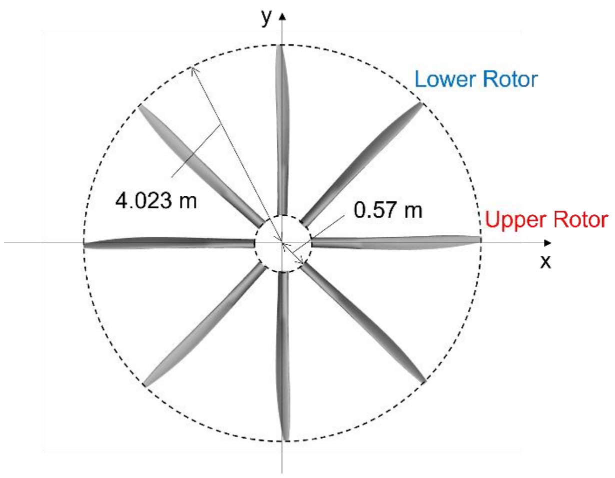

Figure 2: Computational model.

$$LO = \frac{\left|C_{M_x}^U\right| + \left|C_{M_x}^L\right|}{C_T^U + C_T^L} = \frac{r_T}{R} \tag{1}$$

Where R and r_T represent the rotor radius and the radial position of the thrust, correspondingly, while C_{M_x} and C_T stand for the pitching moment and the thrust coefficient, respectively. The subscripts U and L pertain to the upper and lower rotors.

The flow field surrounding a coaxial rotor is very complex, arising from the intricate interplay of vortices and blade interference. Moreover, the interference of pressure fields during blade passage engenders blade vibrations. These aerodynamic interferences significantly contribute to rotor vibration and noise (Ref. 4).

Hayami (Ref. 5) conducted a comprehensive computational fluid dynamics (CFD) analysis on a 2 blades per rotor (N_b = 2) coaxial system, building upon wind tunnel tests by Cameron et all (Ref. 6). The study demonstrated that manipulating the lift offset can effectively mitigate thrust oscillations. However, it was discerned that restraining thrust-induced vibrations becomes progressively challenging with escalating forward flight speeds. Ho et al (Ref. 7, 8). explored the vibrational characteristics of a coaxial rotor, revealing that a blade phase angle shift between the upper and lower rotors can mitigate the vibration within the coaxial rotor system. During the X2 Technology Demonstrator assessments, Walsh et al (Ref. 9). suggested that adjusting the blade displacement angle contributes to the reduction of thrust fluctuations. Nonetheless, a comprehensive understanding of the complex vibration reduction mechanisms and the optimal phase shift angle between the upper and lower rotors remains

Table 1: Specification of the rotor blades.

Number of blades N_b	4
Rotor radius R	4.023 m
Precone angle	2°
Rotor solidity σ	0.1441
Rotor separation	0.4572 m
Rotation	Upper CCW

elusive. Furthermore, the impact of vibration mitigation under high advance rate conditions, specifically $\mu = 0.6$ or higher, has yet to be examined. The advance ratio μ are defined as follows:

$$\mu = \frac{V_\infty \cos i}{\Omega R} \tag{2}$$

where V_∞ and i denotes the freestream velocity and the rotor disk plane incidence angle, respectively.

The primary objective of this study is to delve into the complex mechanisms of vibration reduction and to determine the optimal phase difference angle between the upper and lower rotors under conditions of high advance ratio. This investigation shall be conducted through high fidelity numerical simulations.

2. COAXIAL ROTOR MODEL

Figure 2 shows the computational model used in this study. The model is based on the X2 Technology Demonstrator, developed by Sikorsky in the U.S (Ref. 10). The blades were created by combining five Sikorsky airfoils, DBLN526, SC325218, SC36212, SC36210, and SSCA09. The radius of this model is 4.023 m and the number of blades per rotor N_b = 4. Table 1 summarizes the specifications used in this study.

3. NUMERICAL SIMULATION

3.1. Numerical method

Numerical simulations were performed on JSS3 (JAXA Supercomputer System generation3) using a rotorcraft CFD tool, rFlow3D, developed at the Japan Aerospace Exploration Agency (JAXA). rFlow3D has been validated for prediction accuracy on rotorcraft (Ref. 11, 12, 13, 14). The governing equations are the compressible Navier-Stokes equations, and a moving overlapped grid is applied to simulate the rotor blade motions. The computational grid is

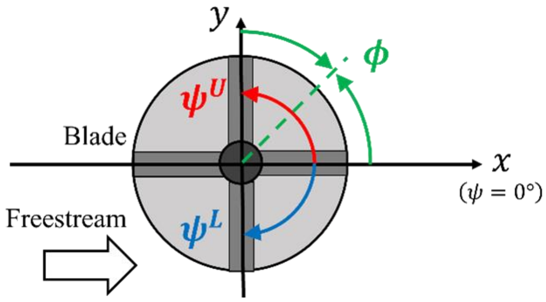

Figure 3: Definition of the azimuth angle, ψ and the inter-rotor phase angle, ϕ.

Table 2: Assumed flight conditions.

Advance ratio μ	0.6, 0.7, 0.8
Lift offset LO	0.3
Gross Weight	5955 lb
RPM	438, 413, 390

discretized using a finite volume method for structured grids. This calculation uses the trim analysis developed by Sugawara et al (Ref. 15). The trim analysis is performed with the pitching moment, torque balance, and rolling moment as target variables, where the lift offset is adjusted based on the target rolling moment.

3.2. Computational setup

The vibration characteristics are investigated at a high advance ratio $\mu = 0.6$~0.8. The tip Mach number of the blade is changed depending on the tip Mach number at the advancing side $M_{\mathrm{Adv,Tip}} \leq 0.9$. The target rotor thrust is set to be the gross weight of X2TD. The target rolling moment of the rotor is determined by the lift offset, which is determined considering the structural limit (Ref. 3), and the pitching moment of the rotor is set to zero. The rotor disk plane incidence angle, i, is set to zero degrees in this study. Figure 3 shows the definition of the azimuth angle, ψ, and inter-rotor phase angle, ϕ. The inter-rotor phase angle is defined as the azimuth angle at which upper and lower rotor blades first cross. Where the inter-rotor phase angle is positive counterclockwise and the subscript U represents the upper rotor, and the subscript L represents the lower rotor. The phase difference between rotors simulates ϕ = 7.5°, 15°, 22.5°, 30°, 37.5°, and 45° to

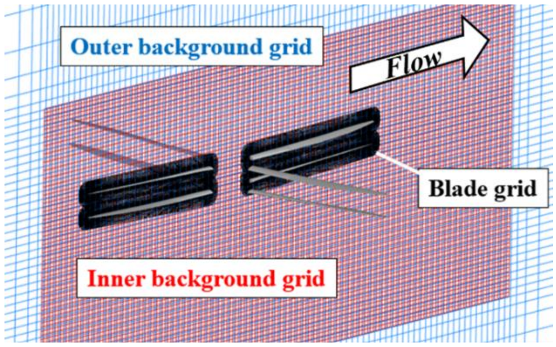

Figure 4: Grid distributions of the coaxial rotor.

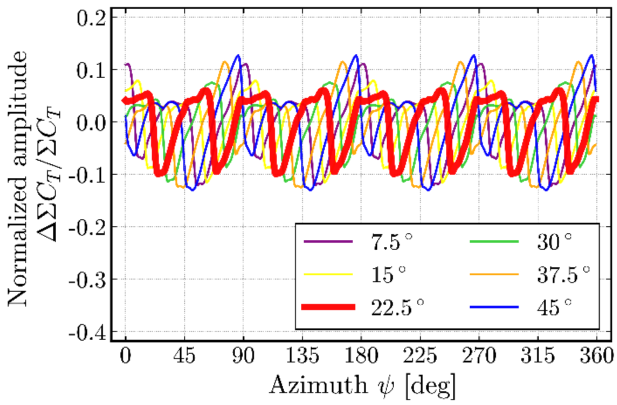

(a) μ = 0.6

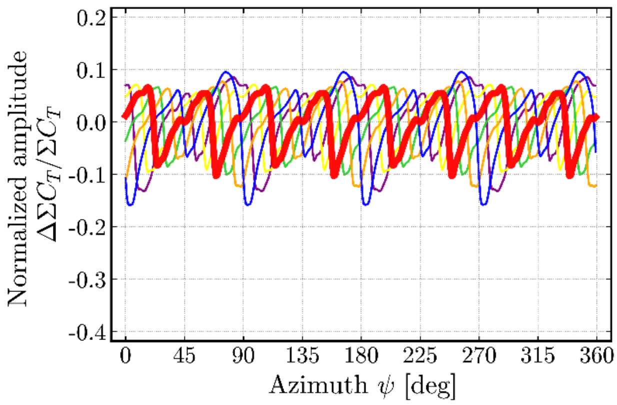

(b) μ = 0.7

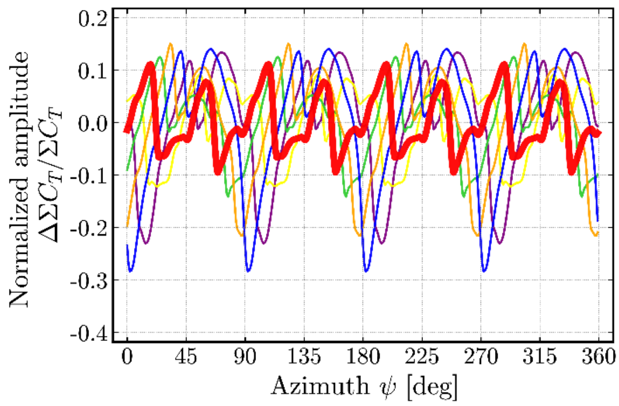

(c) μ = 0.8

Figure 5: Thrust fluctuations for μ = 0.6, 0.7 and 0.8.

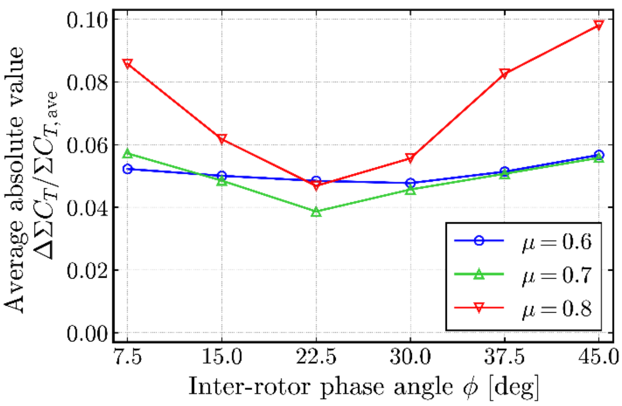

Figure 6: Mean of the absolute value of thrust fluctuations.

investigate the optimum inter-rotor phase angle. Table 2 summarizes the assumed flight conditions in this study.

Figure 4 shows the overlapping grid system used in this study. The total number of computational grid points is about 32 million. The inner background grid has a uniform grid distribution, while outer background grid has non-uniform grid distribution. The grid size of the inner background grid is 15% of the 75%R chord length of the blade.

4. RESULT AND DISCUSSION

4.1. Thrust variation of 4/rev (N_b/rev) component

CFD analyses are performed for the conditions of $\mu \geq 0.6$ to investigate the difference in thrust variation with inter-rotor phase angle, ϕ. Figure 5 shows the thrust fluctuations for $\mu = 0.6$, 0.7, and 0.8, respectively. For the total thrust coefficient, the dimension-less fluctuation is obtained by subtracting the mean value from the value at each azimuth angle and then dividing it by the mean value. Figure 6 shows the mean of the absolute value of thrust fluctuation as a function of inter-rotor phase angle. Figures 6 and 7 show that the thrust fluctuations are reduced even at $\mu \geq 0.6$, with the minimum of thrust fluctuation observed at $\phi = 22.5°$ across all advance ratios.

Figure 7 shows the results of the discrete Fourier transform at each advance ratio. The vertical axis represents the dimensionless amplitude normalized by the average thrust, and the horizontal axis represents the vibration period per rotor revolution. Notably, Figure 7 reveals a remarkable reduction in the

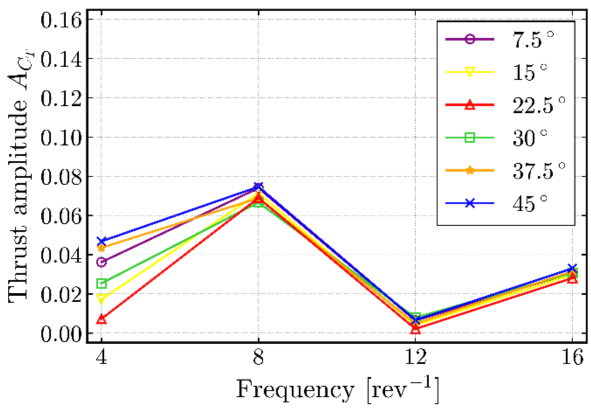

(a) $\mu = 0.6$

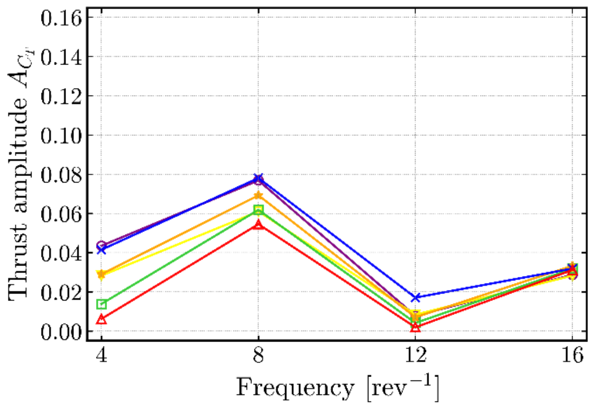

(b) $\mu = 0.7$

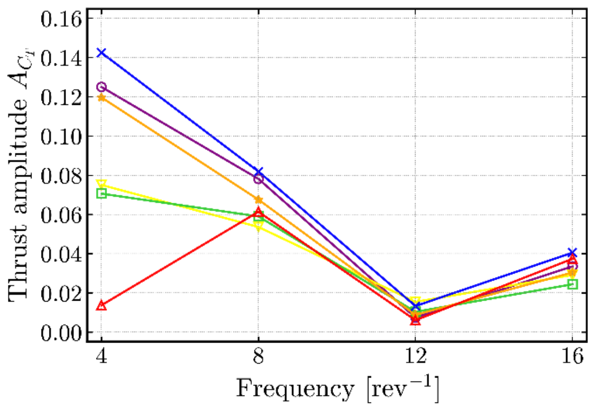

(c) $\mu = 0.8$

Figure 7: Frequency spectra of the total thrust fluctuation for $\mu = 0.6$, 0.7 and 0.8.

Nb/rev vibration component across all advance ratios. Particularly in Figure 7 (c), at $\mu = 0.8$, the N_b/rev component exhibits a staggering decrease of approximately 90%.

Figure 8 shows the discrete Fourier transform results for $\mu = 0.6$, 0.7, 0.8 at ϕ = 22.5°, alongside the thrust variation during hovering. Importantly, Figure 8 demonstrates that even at $\mu \geq 0.6$, the appropriate

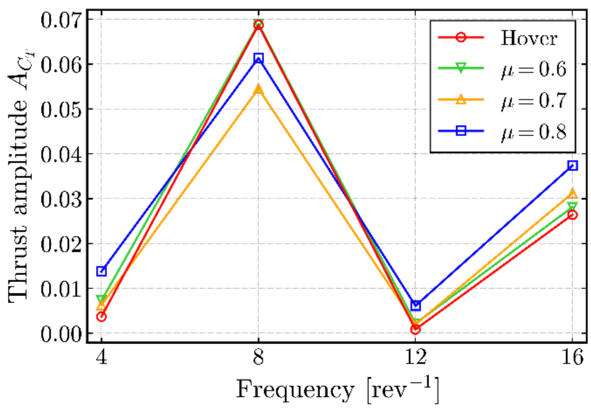

Figure 8: Frequency spectra of the total thrust fluctuation at the ϕ = 22.5°.

inter-rotor phase angle holds the potential to minimize the fluctuation to a level akin to that experienced during hovering.

Figure 9 shows the thrust fluctuations of the upper and lower rotors at μ = 0.8 and LO = 0.3, respectively. Remarkably, Figure 9 indicates that at ϕ = 45°, the N_b/rev thrust variations of the upper and lower rotors harmoniously reinforce one another in phase, while at ϕ = 22.5°, the N_b/rev thrust variations of the upper and lower rotors elegantly cancel each other in opposite phase.

Figure 10 shows the distribution of the vertical force coefficient, $C_n M^2$, on the rotor surface for the sum of the upper and lower rotors. $C_n M^2$ is defined as follows:

$$C_n M^2 = \frac{2 f_z}{\rho_\infty a_\infty^2 c} \quad (3)$$

Where the vertical force is denoted by f_z, air density in the freestream by ρ_∞ , speed of sound in freestream by a_∞ and blade cord length by c.

Figure 10 vividly demonstrates that μ = 0.8 exhibits the most non-uniform lift distribution, while μ = 0.6 displays the most uniform lift distribution. This observed variation arises from the distinct size of the reverse flow region. Despite the expectation that μ = = 0.8 would yield the largest thrust fluctuations, because of the non-uniform lift distribution on the rotor surface, Figure 8 intriguingly showcases similar thrust fluctuations for all advance ratios. Consequently, Figures 8, 9, and 10 collectively underscore

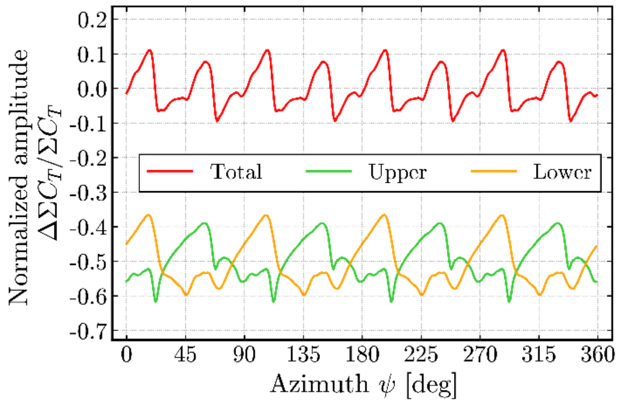

(a) ϕ = 22.5°

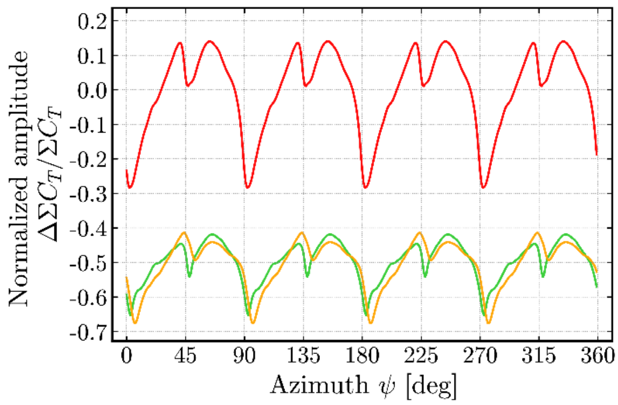

(b) ϕ = 45°

Figure 9: Thrust fluctuations of the upper and lower rotors at μ = 0.8 and LO = 0.3.

that the strategic implementation of the inter-rotor phase angle proficiently mitigates thrust fluctuations to a level equivalent to that experienced during hovering, independent of the lift distribution on the rotor surface.

4.2. Thrust variation of 8/rev (N_b/rev) component

Figure 11 exhibits the $2N_b$/rev thrust variation component as a function of the inter-rotor phase angle for different advance ratios. It becomes apparent from Figure 11 that the $2N_b$/rev thrust variation component diminishes significantly by the inter-rotor phase angle for μ = 0.7 and 0.8, while it remains relatively constant at μ = 0.6.

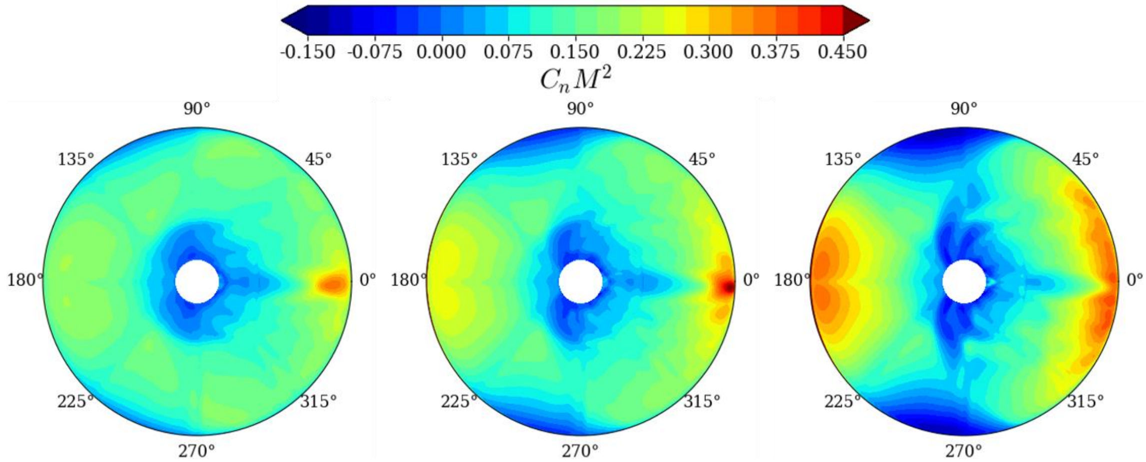

(a) $\mu = 0.6$ (b) $\mu = 0.7$ (c) $\mu = 0.8$

Figure 10: Distribution of $C_n M^2$ on the rotor surface for the sum of the upper and lower rotors.

The $2N_b$/rev thrust variation component emerges because of pressure field interference at the intersection of upper and lower rotor-blades in the coaxial rotor configuration. As revealed in Figure 10, an escalated advance ratio correlates with increased lift generation both ahead and behind of the aircraft. Moreover, Figure 11 implies that the inter-rotor phase angle influences the lift force generated at the intersection of the upper and lower rotor blades.

The magnitude of the pressure field surrounding the blade undergoes variation in tandem with the generated lift, consequently influencing the intensity of interference at the blade crossing (Ref. 16). Considering these observations, it is recommended to optimize the inter-rotor phase angle, such that the lift generated by the upper and lower rotor blades intersects at a smaller azimuth angle. By doing so, the $2N_b$/rev thrust fluctuation component can be effectively diminished.

4.3. Moment variation

In addition to investigating the thrust variation, this study also conducted a comprehensive analysis of the rolling moment coefficient, C_{M_x}, and the pitching moment coefficient, C_{M_y}. These coefficients are defined as follows:

$$C_{M_x} = \frac{M_x}{\rho_\infty \pi R^3 (\Omega R)^2} \tag{4}$$

$$C_{M_y} = \frac{M_y}{\rho_\infty \pi R^3 (\Omega R)^2} \tag{5}$$

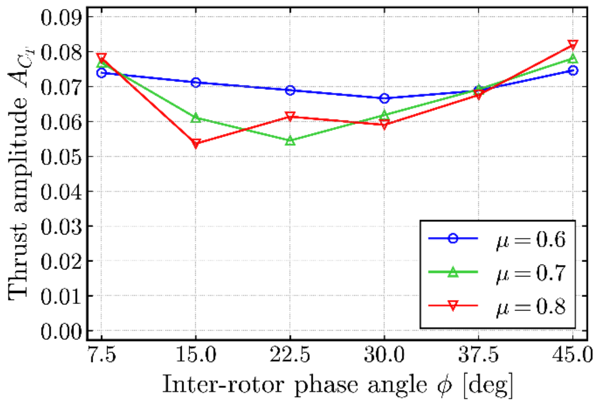

Figure 11: $2N_b$/rev thrust variation component.

Where M_x and M_y denote the rolling moment and pitching moment, respectively.

Figure 12 presents the outcomes of the discrete Fourier transform of C_{M_x} at various advance ratios, while Figure 13 showcases the results of the discrete Fourier transform of C_{M_y} at different advance ratios. Remarkably, Figures 12 and 13 elucidate that the Nb/rev component of C_{M_x} amplifies at $\phi = 22.5°$, whereas the Nb/rev component of C_{M_y} nearly diminishes to zero at the same angle. These variations are intrinsically tied to the non-uniform lift distribution on the rotor surface, as expounded in Figure 10. Significantly, these observed trends align with the experimental findings of Cameron et al. (Ref. 6), and they consistently hold true for high advance ratios and $N_b = 4$.

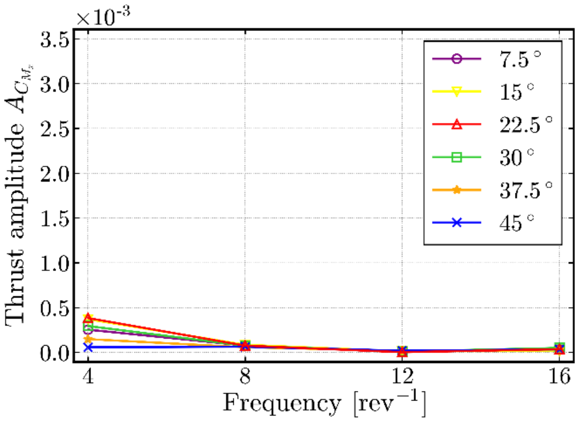

(a) $\mu = 0.6$

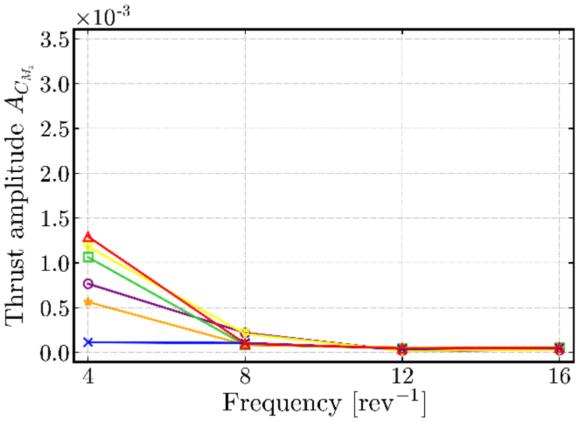

(b) $\mu = 0.7$

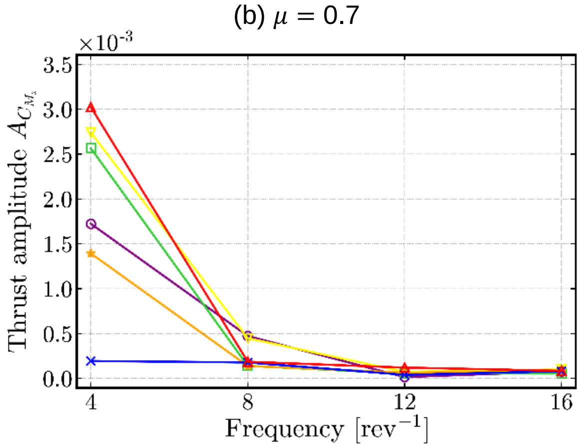

(c) $\mu = 0.8$

Figure 12: Frequency spectra of C_{M_x} for $\mu = 0.6$, 0.7 and 0.8.

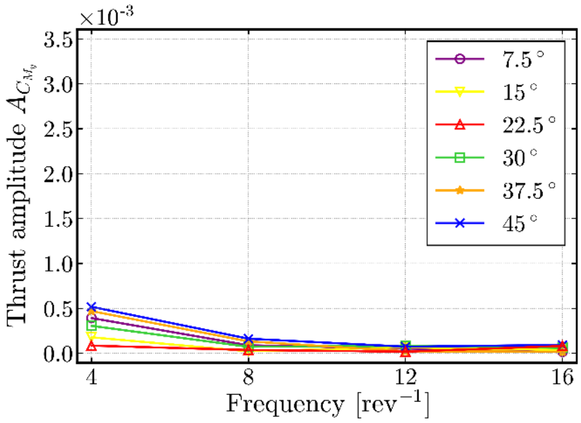

(a) $\mu = 0.6$

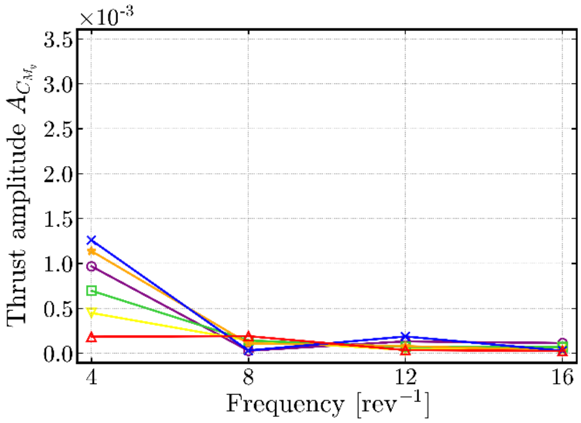

(b) $\mu = 0.7$

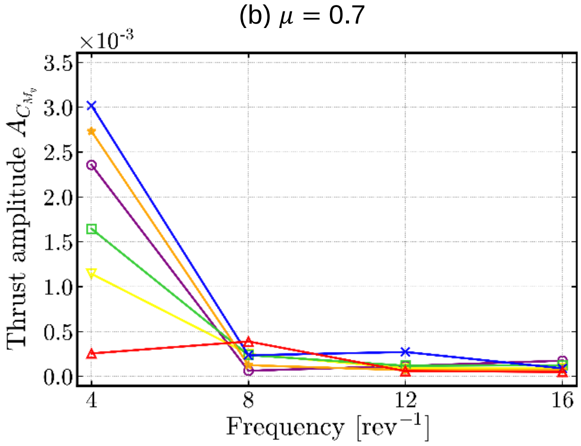

(c) $\mu = 0.8$

Figure 13: Frequency spectra of C_{M_y} for $\mu = 0.6$, 0.7 and 0.8.

5. CONCLUSIONS

This study delves into the influence of inter-rotor phase angle on thrust and moment variation during high-speed forward flight conditions. The Sikorsky X2 Technology Demonstrator's coaxial rotor serves as the model, and Computational Fluid Dynamics (CFD) analysis is employed. Six cases of inter-rotor phase angle ranging from 7.5° to 45° in 7.5° increments were analyzed for $\mu = 0.6$, 0.7, and 0.8 with $LO = 0.3$, respectively. The principal findings are summarized as follows:

1. Setting the inter-rotor phase angle to $\phi = 22.5°$ yields a remarkable reduction in thrust fluctuations, even under high-speed forward flight con-

ditions ($\mu \geq 0.6$), with fluctuations equivalent to those experienced during hovering. This notable outcome can be attributed to the synchronization of vibration phases between the upper and lower rotors in opposite phases, thereby diminishing the N_b/rev thrust fluctuation component by an impressive 90%.

2. The inter-rotor phase angle also leads to a reduction in the $2N_b$/rev thrust fluctuation component. This phenomenon can be attributed to the strategic intersection of the upper and lower rotor blades at an azimuth angle where the generated lift is relatively smaller, consequently resulting in diminished pressure field interference at the crossing point.

3. C_{M_x} and C_{M_y} exhibit opposite trends in response to variations in the inter-rotor phase angle, wherein one parameter diminishes while the other augments. This observed behavior aligns with the findings of the previous study, even under conditions of high advance ratio and $N_b = 4$.

Author contact:

Takumi Yumino t-yumino@st.go.tuat.ac.jp

6. REFERENCES

1. Yeo, H., Johnson, W., "Optimum Design of a Compound Helicopter", JOURNAL OF AIRCRAFT Vol. 46, No. 4, July–August2009.

2. Ruddell, A. J., Growth, W., McCutheon, R., "Advancing Blade Concept (ABC) Technology Demonstrator", ADA100181, 1981.

3. Bagai, A., "Aerodynamic Design of the X2 Technology Demonstrator™ Main Rotor Blade", American Helicopter Society 64th Annual Forum, Vol. 64, p. 29, 2008.

4. Passe, B., Sridharan, A., Beader, J., "Computational Investigation of Coaxial Rotor Interactional Aerodynamics in Steady Forward Flight", 33rd AIAA Aerodynamics Conference, 2015.

5. Hayami, K., Sugawara, H., Yumino, T., Tanabe, Y. and Kameda, M., "CFD Analysis on the performance of a coaxial rotor with lift offset at high advance ratio," Aerospace Science and Technology, 2023.

6. Cameron, C., Sirohi, J., "Performance and Loads of a Model Coaxial Rotor Part I: Wind Tunnel Testing", American Helicopter Society 72nd Annual Forum, 2016.

7. Ho, J., Yeo, H., "Analytical study of an isolated coaxial rotor system with lift offset", Aerospace Science and Technology 100-2020-105818, 2020.

8. Ho, J., Yeo H., "Rotorcraft Comprehensive Analysis Calculations of a Coaxial Rotor with Lift Offset", International Journal of Aeronautical and Space Sciences, 2020.

9. Walsh, D., Weiner, S., Arifian, K., Lawrence, T., Wilson, M., Millot, T., Blackwell, R., "High Airspeed Testing of the Sikorsky X2 Technology™ Demonstrator", 67th Annual Forum of the American Helicopter Society International, 2011.

10. Walsh, D., Weiner, S., Arifian, K., Bagai, A., Lawrence, T., Blackwell, R., "Development Testing of the Sikorsky X2 Technology™ Demonstrator", 65th Annual Forum of the American Helicopter Society International, 2009.

11. Tanabe, Y., Saito, S., "Significance of all-speed scheme in application to rotorcraft CFD simulations", Proceedings of 3rd International Basic Research Conference on Rotorcraft Technology, p. 23, 2009.

12. Tanabe, Y., Saito, S., Takayama, O., Sasaki, D., Nakahashi, K., "A new hybrid method of overlapping structured grids combined with unstructured fuselage grids for rotorcraft analysis", Proceedings of 36th European Rotorcraft Forum, p. 071, 2010.

13. Tanabe, Y., Saito, S., Sugawara, H., "Evaluation of rotor noise reduction by active devices using a CFD/CSD coupling analysis tool chain", proceedings of 1st Asian/Australian Rotorcraft Forum, pp. A-IV-1-P107-F, 2012.

14. Tanabe, Y., Saito, S., Sugawara, H., "Construction and validation of an analysis tool chain for rotorcraft active noise reduction", Proceedings of 38th European Rotorcraft Forum, pp. ERF2012–025, 2012.

15. Sugawara, H., Tanabe, Y., Kameda, M., "A coupled CFD/Trim Analysis of Coaxial Rotors", Trans. Japan Soc. Aero. Space Sci. Vol. 65, No. 6, pp. 262-272, 2022.

16. Hayami, K., Sugawara, H., Tanabe, Y, Masaharu, K., "Numerical Investigation of Aer-

odynamic Interference on Coaxial Rotor”, AIAA
Scitech 2020 Forum, AIAA, 2020